Received: 7 October 2022 | Revised: 25 August 2023 | Accepted: 30 September 2023

DOI: 10.1111/ter.12691

RESEARCH ARTICLE

Terra Nova WILEY

The micro-seismicity of Co. Donegal (Ireland): Defining baseline seismicity in a region of slow lithospheric deformation

Federica Riva[1,2] | Nicola Piana Agostinetti[2] | Simone Marzorati[3] | Clare Horan[4]

[1]School of Advanced Studies, University of Camerino, Camerino, Italy

[2]Department of Earth and Environmental science, University of Milano-Bicocca, Milan, Italy

[3]Centro Nazionale Terremoti, Istituto Nazionale di Geofisica e Vulcanologia (INGV), Ancona, Italy

[4]Geophysics Section, Dublin Institute for Advanced Studies, Dublin, Ireland

Correspondence
Federica Riva, School of Advanced Studies, University of Camerino, Camerino, Italy.
Email: federica.riva48@gmail.com

Funding information
Science Foundation Ireland, project SIM-CRUST, Grant Number 11/SIRG/E2174

Abstract

A catalogue of precisely located micro-seismicity is fundamental for investigating seismicity and rock physical properties in active tectonic and volcanic regions and for the definition of a 'baseline' seismicity, required for a safe future exploitation of georesource areas. In this study, we produce the first manually revised catalogue of micro-seismicity for Co. Donegal region (Ireland), an area of about 50$K\,M^2$ of on-going deformation, aimed at localizing natural micro-seismic events occurred between 2012 and 2015. We develop a stochastic method based on a Markov chain Monte Carlo (McMC) sampling approach to compute earthquake hypocentral location parameters. Our results indicates that micro-seismicity is present with magnitudes lower than 2 (the highest magnitude is 2.8).The recorded seismicity is almost clustered along previously mapped NE-SW trending, steeply dipping faults and confined within the upper crust (focal depth less than 10 km). We also recorded anthropogenic seismicity mostly related to quarries' activity in the study area.

KEYWORDS
catalogue, Donegal granite region, geothermal research, *micro-seismicity*, Monte Carlo sampling solution

1 | INTRODUCTION

The Co. Donegal region is located in the northwestern part of Ireland, and it is part of the NE-SW trending Caledonian fold belt of Lower Palaeozoic age. The major tectonic feature of the area is the presence of the NE-SW trending fault system, of which the Leannan Fault is the most representative example. The Leannan fault is directly in line with the Great Glen fault and the possibility that it is a north-west continuation of this structure is discussed (Pitcher et al., 1964). Ireland is a region of slow lithospheric deformation and at the present Co. Donegal is the only seismically active area in Ireland, with an average rate of 1 Mw = 2–3 event every 3–4 years. Regions of slow lithospheric deformations are characterized by a low seismicity rate and limited accumulation and release of tectonic energy, leaving open the question if such deformation is 'diffusely' accommodated along a wide fault system (or even across the whole crust) rather than clusterized along specific faults. In particular, the sparsity of the seismic networks (common in region with low seismic risk) makes it appear, in current catalogue, that seismicity is generally diffuse, but it could also be grossly mislocated due to the small amount of seismic data available. Well-planned experiments with an appropriate density of seismic stations are required to register and locate small events. Otherwise, standard national seismic networks with a low density of seismic stations could not be able to register

Federica Riva equally contributing author.

the target events. Precise location can be achieved through visual inspection of seismic waveforms and manual picking of P- and S-direct phases, where automatic methods should be favoured only in case of large (>10,000 events) catalogue, due to their proness in detecting false-positive cases (Münchmeyer et al., 2022). In addition to the detailed seismic monitoring through dense network, the adopted location procedure has strong impact on the location of events and on the discrimination between natural and human-induced events (also based on the hypocentral depth), therefore on the assessment of the ordinary background micro-seismicity within 1D volume.

Co. Donegal is also the site of post-orogenic radiogenic granites partly exposed along the NW Atlantic coast and potentially buried at shallow depth in the eastern part of the study region. For this reason, the area represents a target for deep (0–5 km depth) geothermal investigation (Goodman et al., 2004). Having a high quality of precisely located micro-seismicity is fundamental before the exploitation of geo-resources for two main reasons. First, seismic waves generated by local events bring information useful to reconstruct the 3D seismic properties of the Earth's crust beneath the seismic network and to better constraint the rock volume in which secondary porosity and fluid circulation may be present. Second, the definition of a 'baseline' seismicity for the area where the exploitation will be in place is necessary to keep the seismic risk related to the exploitation itself under strict control.

For these two reasons, the final aim of our work is the precise location of both human-induced and natural micro seismic events

Significance statement

This work provides the first-ever catalogue of manually revised micro-seismicity of Co.Donegal, a region of ongoing slow lithospheric deformation. Through our work, we tried to give an answer, with a newly developed algorithm, to the open question whether the deformation in these kinds of regions is "diffusely" accommodated within the whole crust rather than clusterized along specific faults.

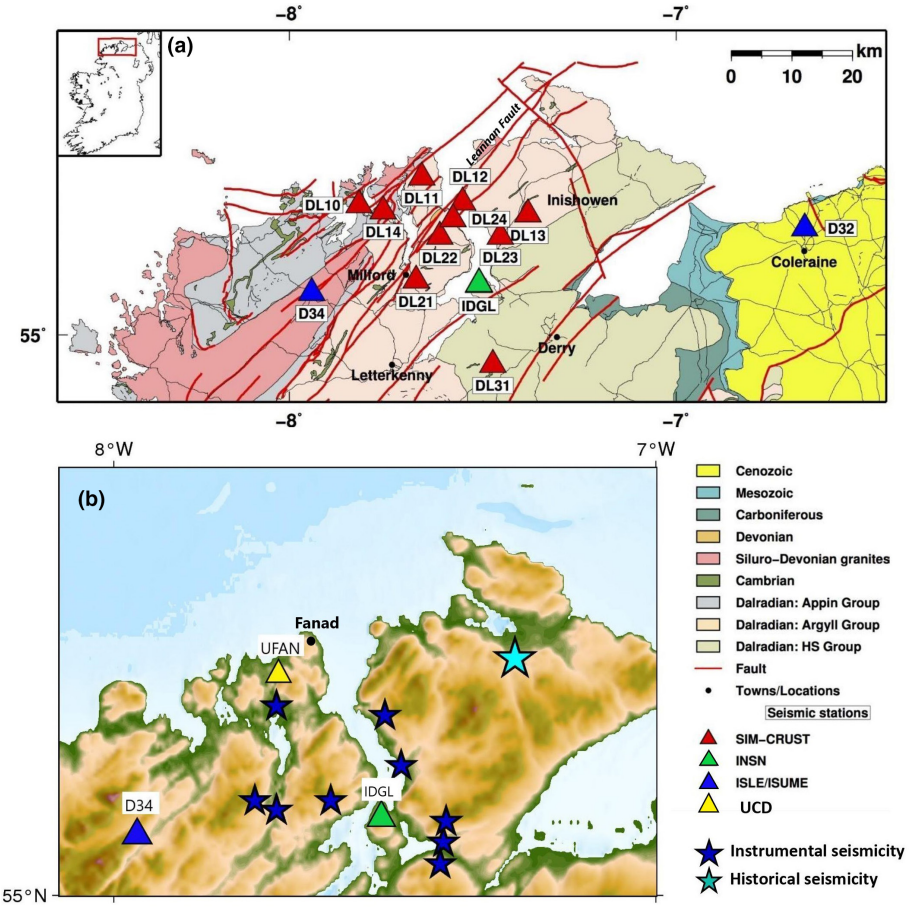

FIGURE 1 (a) Seismic network deployed in Donegal in the framework of the SIM-CRUST project. 12 broadband seismic stations have been deployed for about 2.5 years of continuous recording. Two stations belong to a previous temporary seismic network, ISLE/ISUME projects. Seismic data have been integrated with data from the permanent seismic station IDGL, Irish National Seismic Network. Interstation distance is less than 10 km in the central area. Sources of anthropic noise are present in the area, lowering the quality of the seismic signal recorded. Fault traces in the region are reported as red lines. Colours indicate different terranes. From Agostinetti and Licciardi (2015), courtesy of Andrea Licciardi. (b) Historical and Instrumental seismicity recorded in Donegal region. Seismic stations D34, UFAN and IDGL used to locate the seismic sequence of 2012.

of Co. Donegal, which could give new insights in the tectonic deformation mechanisms and help to find out granite volumes characterized by micro-fractures suitable for fluid circulation. The seismic data provided in this paper have been collected thanks to the SIM-CRUST project: '*Seismic imaging and monitoring of the upper crust: exploring the potential of low-entalphy geothermal resources of Ireland*' (sim-crust.dias.ie). The project comprises the development of two high-density (inter-station distance <10 km) seismic networks to explore the Dublin basin and the Donegal granite region, case of study of our research. Additional seismic data, for a small seismic sequence occurred few months before the deployment of SIM-CRUST stations have been analysed for a more complete picture of the seismicity in the area. These data have been provided by a temporary project (Readman & O'Reilly, 2022) operated by the University College Dublin. Our study focuses on the detection and location procedure through a Markov chain Monte Carlo approach of both natural and human-induced seismicity recorded from August 2012 to July 2015 by 12 broadband seismic stations. We compile a first manual-revised catalogue of Donegal micro-seismicity, and we integrate it with the location of the seismic events occurred in a small seismic sequence during January 2012 in the study area (see Figure 1).

2 | DATA AND METHODS

Within the SIM-CRUST project a seismic network of 12 stations has been installed and maintained in the Co. Donegal from August 2012 to June 2015 (1.a) with the inter-station distance between 5 and 20 km. All stations were equipped with broadband seismometers (Guralp CMG-40T), with a flat response between 50 Hz and 60s. Seven Earth Data PR6-24 Portable Field Recorders have been used, together with four Guralp CMG-EAM Flexible data acquisition modules. Due to the limited space available for storing the digitizer, a Nanometrics Taurus has been installed at station DL13. All stations (except for DL21 and DL13) have been installed within a building allowing for continuous power supply. Continuous waveform data have been archived as 1-day MSEED files at DIAS (Dublin Institute for advanced Studies).

In order to detect the seismic events we analysed the continuous waveforms by applying a STA/LTA network coincidence trigger algorithm (Team, 2017) and using Jupyter Notebook (Executable Books Community, 2020). Then, we performed a manual picking of P and S waves first arrival times of the events detected by the trigger algorithm (Goldstein & Snoke, 2005) for a total of 35 natural events and 79 human-induced events. In order to recover as many phases/events as possible, we varied the STA/LTA parameters several times to find the more reasonable ratio between true triggered events and fake events given by the natural seismic noise. We reviewed all the arrival times to exclude erroneous ones. We also integrated seismic data recorded by other three temporary seismic stations installed during a small seismic sequence occurred in January 2012 near the Fanad peninsula (Möllhoff & Bean, 2016). The seismic sequence was triggered by a Mw 2.5 event occurred next to Milford and has been felt by the local population (https://www.irishtimes.com/news/donegal-earthquakes-homes-1.694869). Finally, a total of 114 earthquakes were located using a hierarchical Bayes Markov chain Monte Carlo (McMC) algorithm. The used McMC algorithm has been developed on purpose for this study and described in detail in Appendix A. The Markov chain Monte Carlo (McMC) method allows us to estimate the realistic uncertainties on the investigated parameters (Lomax et al., 2000). Establish realistic uncertainties is fundamental to robustly relate retrieved earthquake locations to other geological/geophysical observations. The strength of McMC method lies on the fact that the data uncertainties are also considered as part of the unknowns and are robustly estimated through the McMC sampling following a Hierarchical Bayes approach (Malinverno & Briggs, 2004). Moreover, a detailed velocity model of the investigated area does not exist at the moment. This aspect can be easily solved by using our method because we just need to specify the minimum and maximum values of all the priors to define the prior probability distribution (i.e. the velocities of P and S waves). Earthquake locations were represented in map view and cross-section by using GMT (Generic Mapping Tool) and its Python extension PYGMT (Wessel et al., 2019).

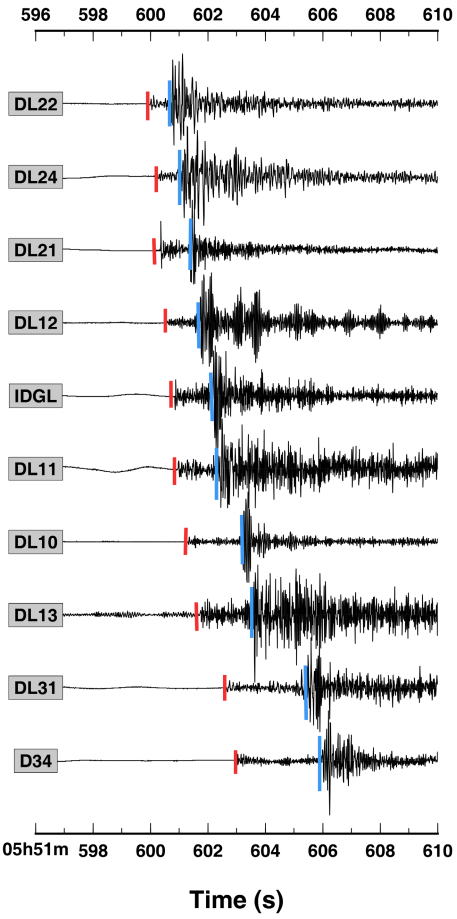

FIGURE 2 Vertical waveform plot for the natural event # 31 with waveforms sorted by arrival times at the stations. P and S onsets are clearly visible.

The seismic network recorded both natural earthquakes and quarry blast events. In the following paragraph, we report the processing and results of two representative events: natural event # 31 and anthropic event # 15. Figure 2 shows the plot for the natural event # 31 after the picking phase sorted by arrival times at the stations. The event is well recorded on all the seismic stations of the network, where the onset of P and S waves are clearly recognizable from the seismic noise of the traces.

Stations DL31, D34, DL10 and DL13 lie on the external perimeter of the seismic network, mostly covering all azimuth directions. At these stations, the Ts-Tp time of all the natural events detected lies in the range 1.5–3 s. This means that the source of all the events must be approximately at the same distance from these stations, leading to a clustered behaviour of all the natural events in the near centre of the network, as reported in 9.

The anthropic event is shown in Figure 3a. The typical waveform of the anthropic events detected is characterized by an initial clear P-wave onset, whereas the S-wave onset is less or no visible on the traces. A relatively long coda occurs at high frequency. Two distinct low-frequency arrivals can be found in the coda of such kind of events (Figure 3b). These patterns are widely recognized in anthropic seismicity (Korrat et al., 2022) (Saadalla et al., 2023) and can be used to classify the artificial events. We also performed a comparative spectral analysis between a natural earthquake and an artificial seismic signal. Natural and human-induced seismic events have different spectral content, and this feature has been used for a correct classification in doubt cases. In Figures 4 panel a) and b) we selected a window of 5 s of noise for both events and in panel c) and d) we selected only the blast and natural waveform to analyse their frequencies content. The spectrum of the blast events is characterized by lower frequencies content and a sharply decrease with increasing frequencies. On the contrary, the natural event is characterized by a more stable pattern of frequencies (Figure 5).

3 | RESULTS

Figure 6 shows the sampled locations of the ML = 1.5 natural event # 31 in map view (panels a and c) and cross-section (panel b). The pink

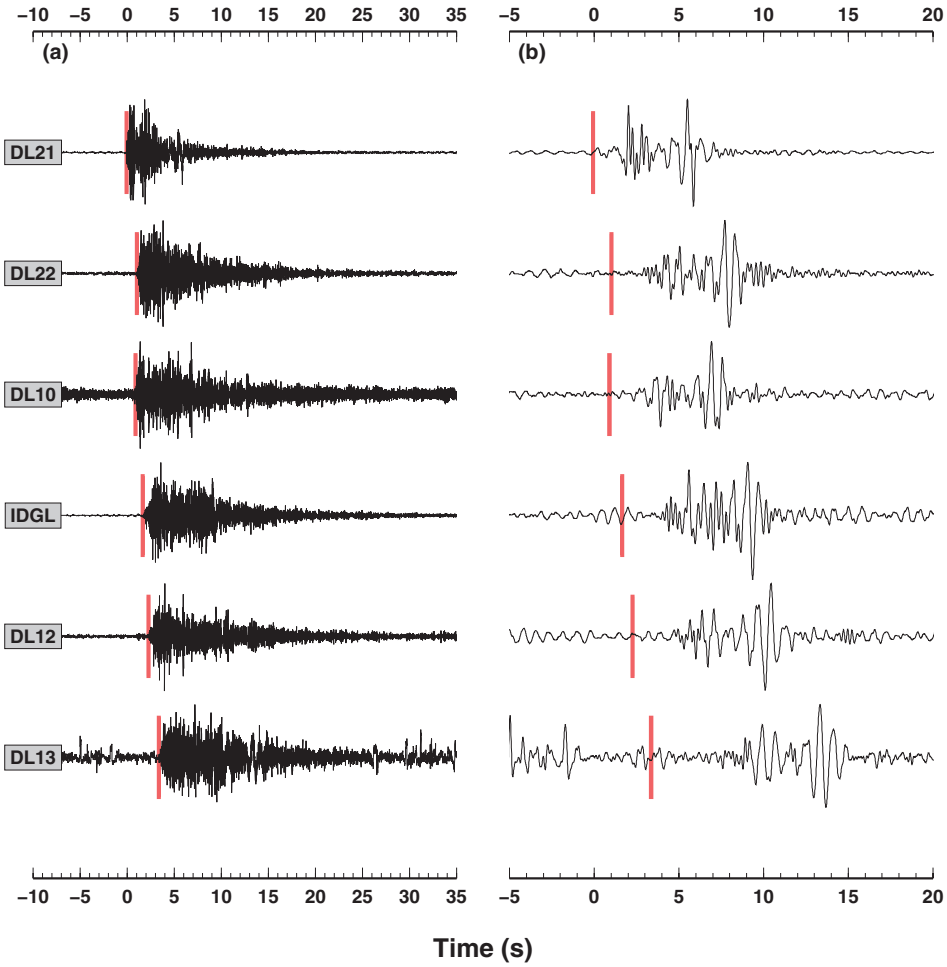

FIGURE 3 (a) Vertical waveform plot for the blast event # 15 with waveforms sorted by arrival times at the stations. P-wave onset is clearly visible (red bars), S waves are less or no distinguishable. (b) same as in (a), but waveforms are filtered with a band-pass filter with corner filter at 1 and 5 Hz.

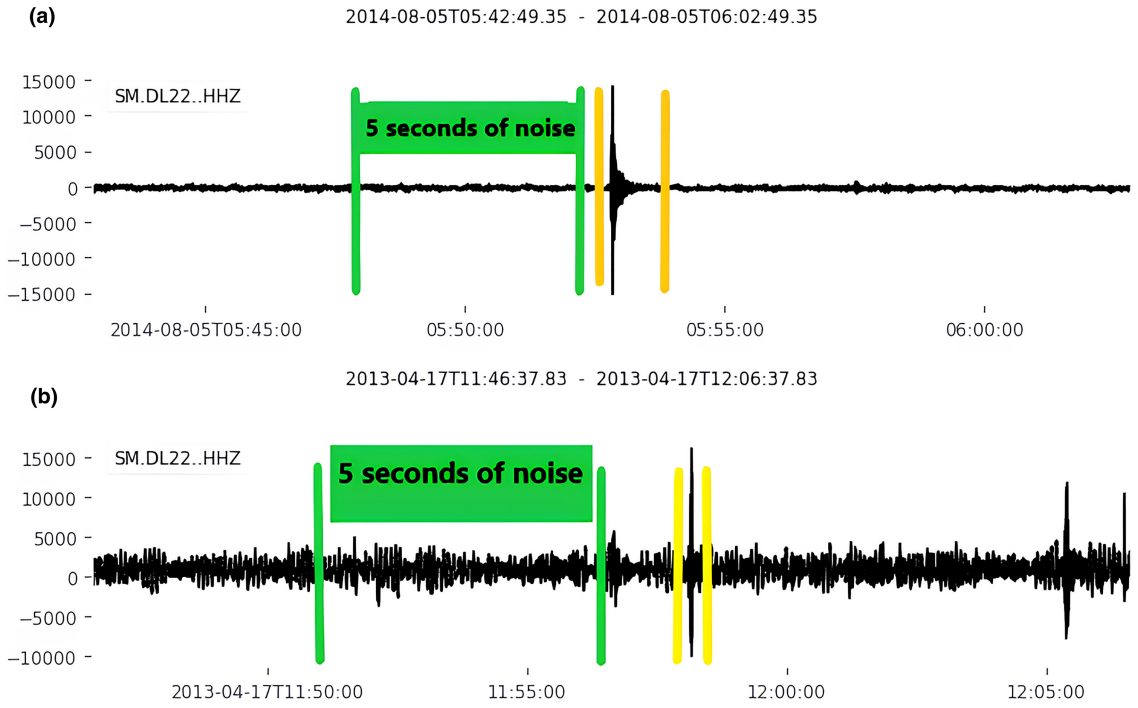

FIGURE 4 20-s trace including: (a) the natural events #31; (b) the blast event #15. Analysed events are indicated with yellow bars.

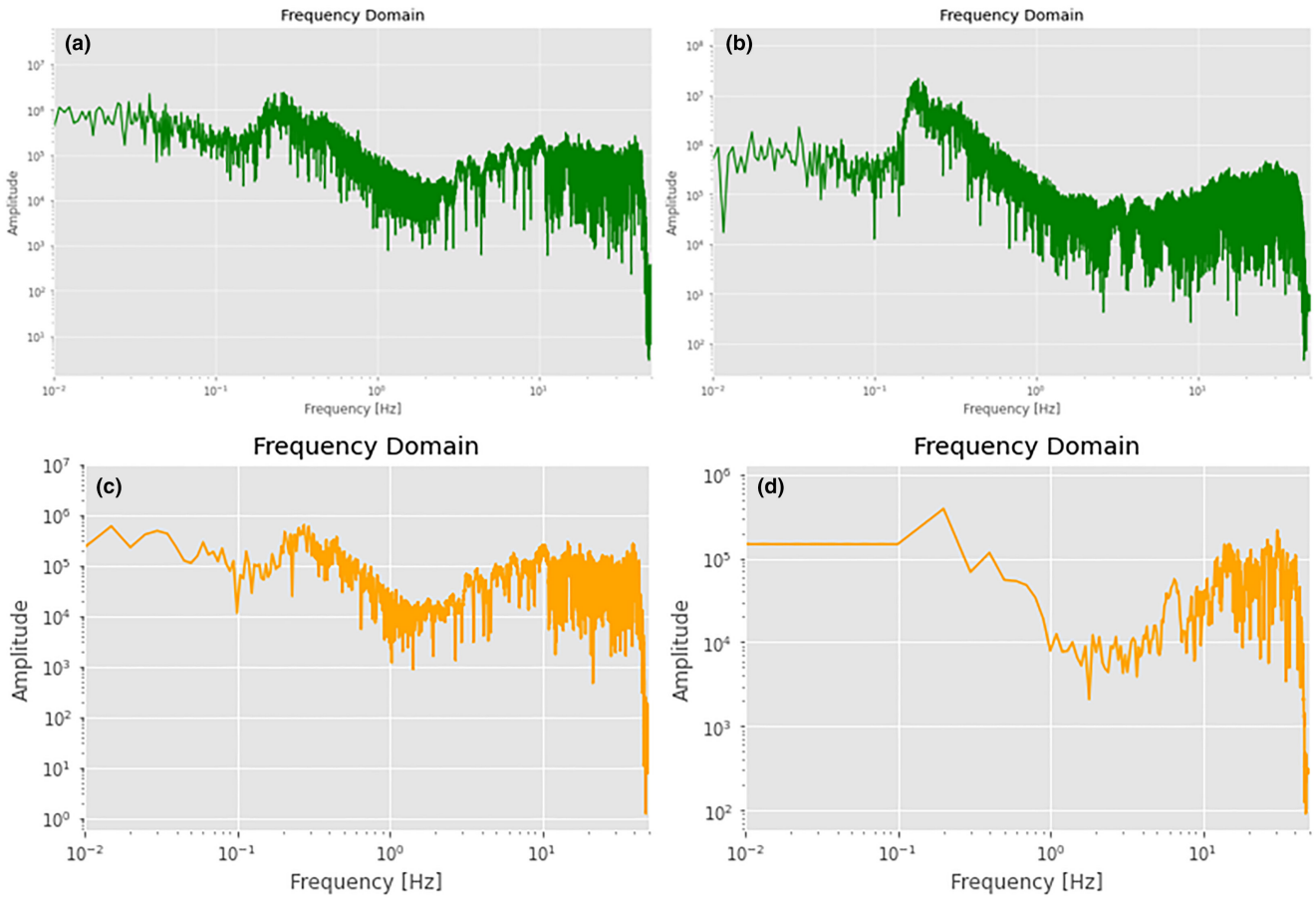

FIGURE 5 Spectrum of 5 s of noise before the natural event (a) and blast event (b). Spectrum of the natural event #31 (c) and blast event #15 (d).

star represents the mean posterior location, and the grey points are all the models collected in the McMC sampling. The epicentral location is well-constrained with a quasi-circular distribution of solutions in the X-Y plane and radius smaller than 1 km (Figure 6c), while the depth is less constrained as shown by the larger spread of solutions with depth (Figure 6b).

We tested the performance of McMC algorithm statistically through frequency distribution histograms; in Figure 7 we show these histograms for event 31. The X and Y parameters show a Gaussian distribution with a standard deviation of about 1 km. The Z parameter (depth value) shows a Gaussian distribution with a mean value at around -7 ± 3 km (Figure 7a–c). The velocity of P waves shows a Gaussian distribution with an average value between 5 and 6 km/s, whereas the velocity of S waves has the highest peak at 3.5 km/s with a standard deviation of about 1 km/s (Figure 7d,e). Both P (π_P) and S wave uncertainties (π_S) have been well-constrained. Their curves show a Gaussian distribution with a narrow shape. The average value for π_P is 1.2, for π_S is 1.4, both with standard deviation lower than 1 (Figure 7g,h). Finally, the mean value for the V_P / V_S ratio is between 1.68 and 1.70 with a standard deviation of less than 0.1.

Figure 8 shows the seismicity recorded during the small seismic sequence occurred in Fanad during January 2021. Seismic data have been recorded by station UFAN, deployed by University College Dublin during the *WaveObs project* (Möllhoff & Bean, 2016). Waveforms for the mainshock and aftershocks display a strong similarity (Figure 8a) with an almost constant S-P time, indicating a common source region. P waves have a clear onset and can be located with precision using standard approaches (Figure 8b).

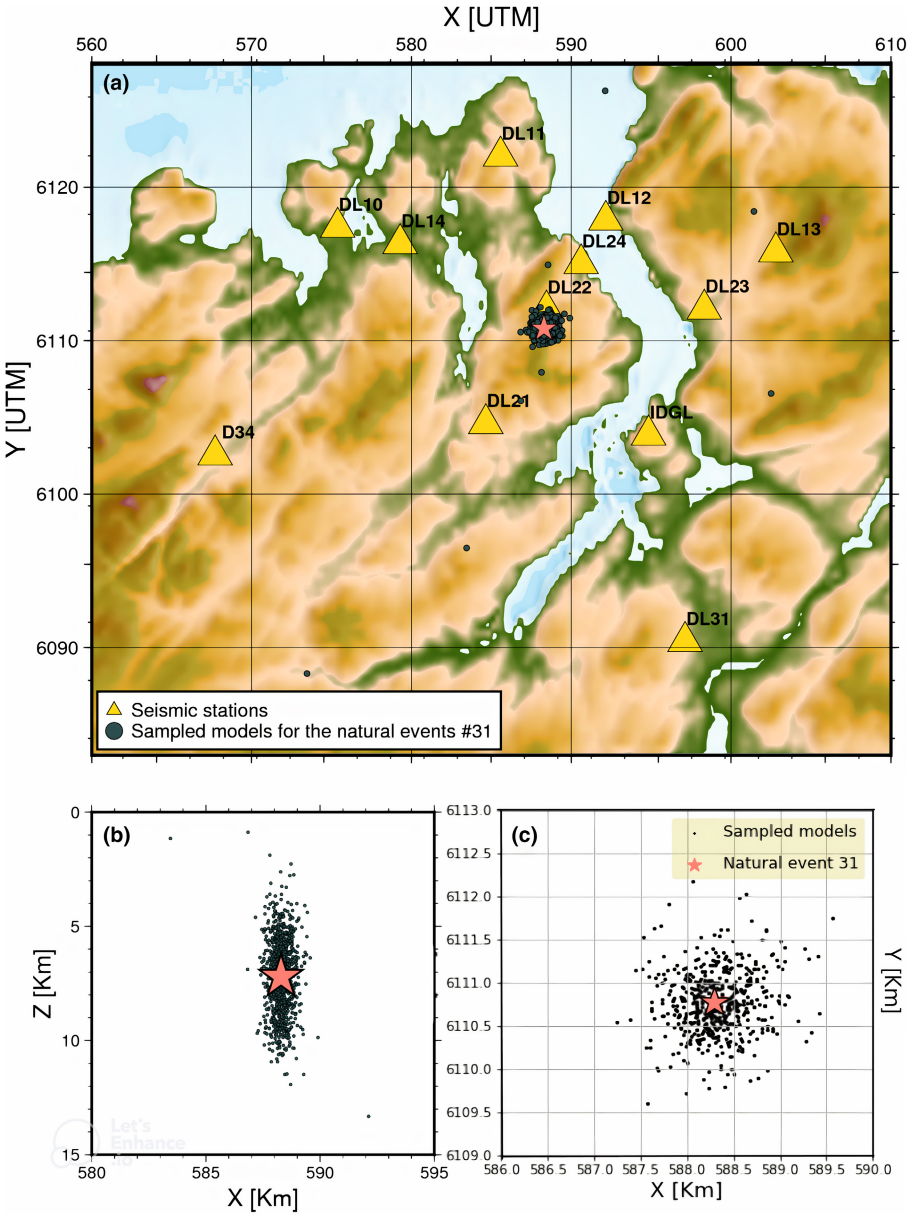

FIGURE 6 Results for event # 31: collected solution during McMC sampling (black dots), with mean posterior location (pink stars). (a) Map view on a X-Y plane. (b) Vertical section on the X-Z plane. (c) Zoom on the map view along the X-Y plane.

Figures 9 and 10 show the final maps of the natural and human-induced events that have been located. The initial total number of detected events to be located was 203: 141 were classified as blast, considering the features described in section 'Methods', 58 as natural events and 4 regional events that have not been considered in the location procedure. After a first location, the events with uncertainties on X and Y parameters >1 Km were eliminated from the catalogue. The high uncertainties of these events may be caused by errors in the detection of real events or uncertainty during the manual picking. For this reason, the total number of events in the final catalogue and shown in the maps 9 and 10 decreased from 203 to 114: 79 are blast events and 35 are natural events.

Figure 9 shows the located natural events within the Donegal Granite region. The natural seismicity is gathered between 55.12 and 55.22 N and between −7.59 and −7.74 E (580–590 Km on the X coordinate and 6110–6120 Km on the Y coordinate) (Figure 9a). In the lower panel (panel b), the events are shown in cross-section along the track line A-B. The majority of the events is clearly aligned, showing a trend towards SE with a high dip angle.

Figure 10 shows the distribution of located blast events within the Donegal area. Most of the blast events are concentrated in the proximity of active local quarries in the area. Table 1 resumes the geographical locations for the Donegal's quarries. Quarries locations have been used to cross-validate the location of the recorded blast events. Comparing the position of the quarries and the clusters of localized blast events, the correlation between the two is clearly visible. This means that the majority of the anthropic events in Donegal are quarry blasts and they have been correctly localized by McMC procedure to their correspondent quarry (Table 2).

3.1 | Local magnitude

We calculated the local magnitude for the natural events located in Co. Donegal as reported in Table 3. Due to the scarceness of local seismicity and the consequent difficult calibration of existing magnitude values with respect to ours, we decided to use two different approaches for magnitude comparison. We first calculated the

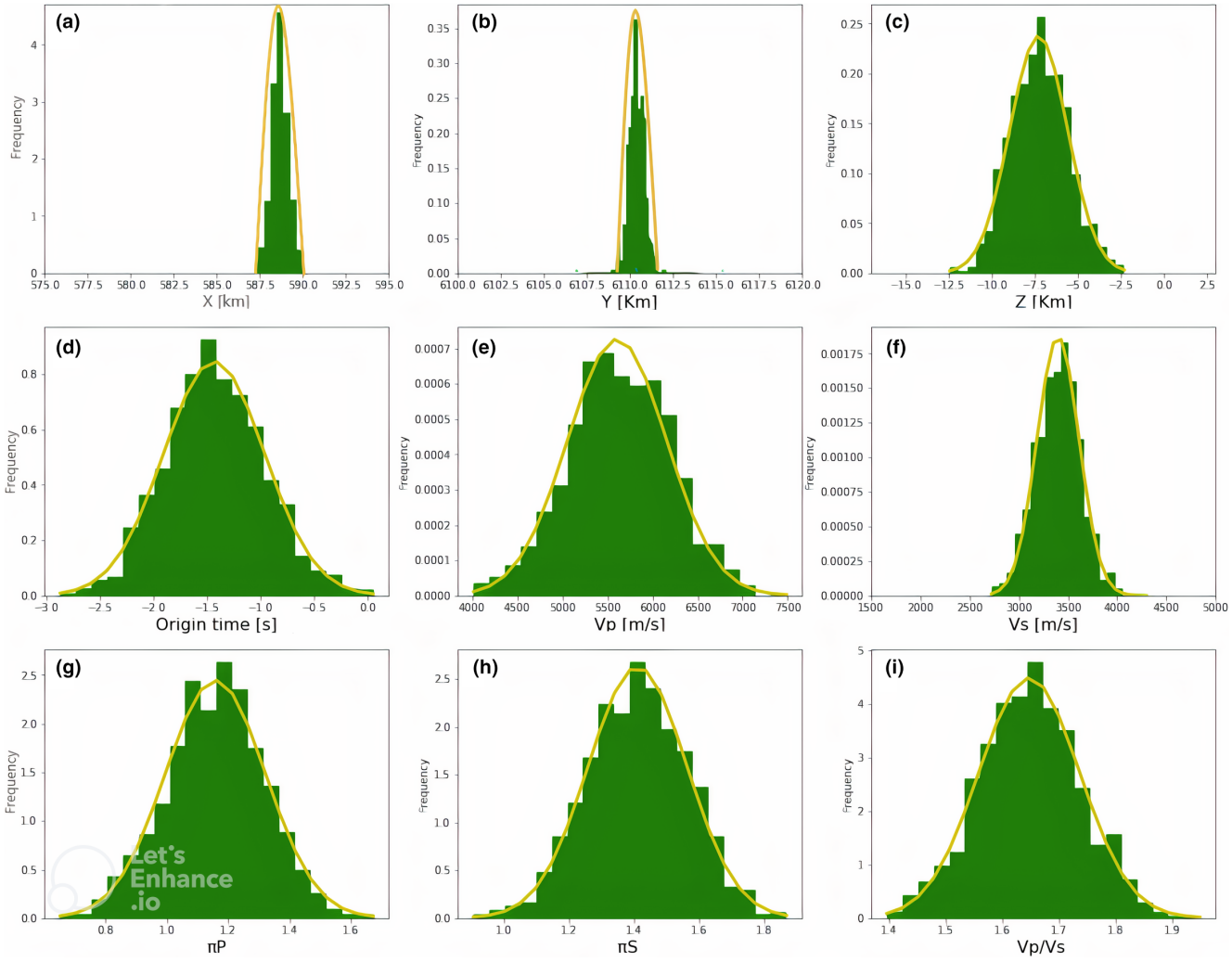

FIGURE 7 Gaussian distributions of (a) longitude [Km] (b) latitude [Km] (c) depth [Km] (d) origin time [s] (e) P-wave velocity [m/s] (f) S-wave velocity [m/s] (g) uncertainty related to the P-wave picking (h) uncertainty related to the S-wave picking (i) P- and S-wave velocity ratio.

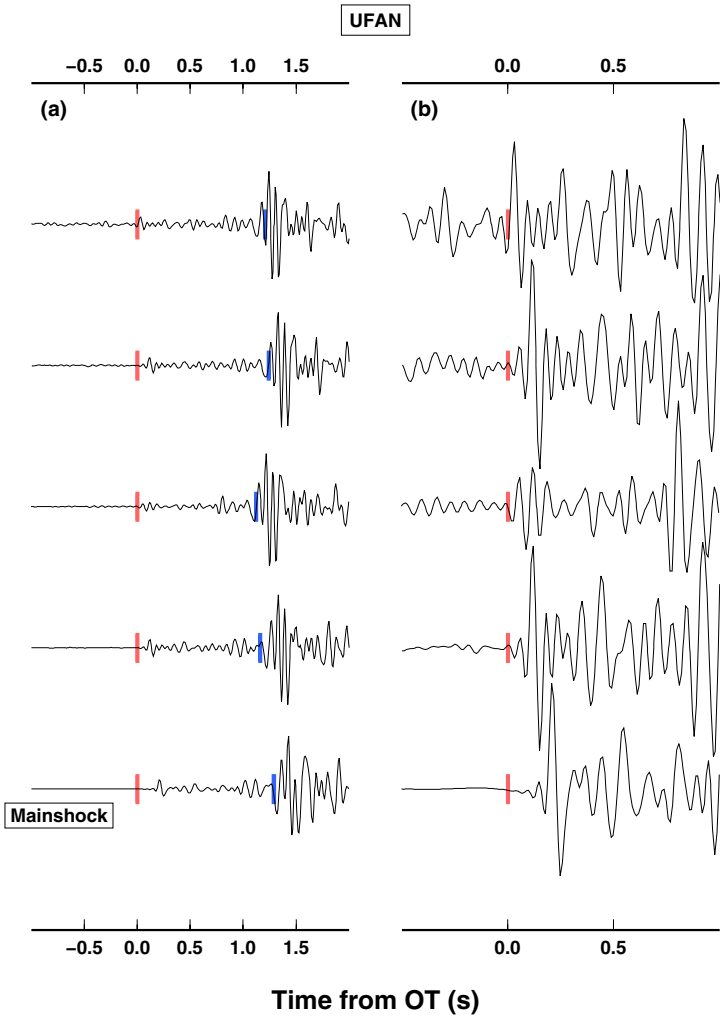

FIGURE 8 Natural event belonging to the 2012 sequence registered at the UFAN seismic station. (a) P-wave onset (red bar) and S-wave onset (blue bar). (b) Zoom on the first P-wave arrivals for all the events. P-wave onset is clearly detectable on all events.

individual magnitude at each station using the following formula by Richter (1935):

$$ML = \log_{10}(A) - \log_{10}(A0) \quad (1)$$

being ***A*** the measured ML Wood-Anderson amplitude in millimetres. The second member is the empirical calibration function, which in turn is a function of the epicentral distance (Richter, 1935). This formula applies the updated Woods-Anderson parameters (gain = 2080, natural period T0 = 0.8 s and damping constant h = 0.7). We then calculated the magnitude at each station using a calibrated local scale for Ireland, provided in the study of Grannell et al., 2018 following the formula:

$$ML = \mathrm{Log}(A) - \mathrm{Log}(A0) + S \quad (2)$$

where ***A*** is the maximum amplitude of the earthquake *S* wave on a Wood-Anderson filtered trace, ***S*** is a station correction coefficient and **Log(*A0*)** is a distance-dependent correction term accounting for geometrical spreading and anelastic attenuation resulting from this equation:

$$\mathrm{Log}(A0) = -a^{*}\log(R) - b^{*}R - c$$

with $a = 1.095717$, $b = 0.001552$ and $c = -2.028571$ and R is the hypocentral distance. We added a stations correction term for the individual station used by the Irish Seismic Network and provided in the study of Grannell et al., 2018 for both Formulas (1) and (2). We then averaged the individual ML values for each station. However any individual ML measurement that was more than two standard deviations from the mean ML value was discarded, and then the average ML was recalculated. We used this criterion for both approaches. The following Table reports the coefficients of the seismic stations used in this study and applied to Equations (1) and (2):

Table 3 reports the final magnitude values for the 35 natural seismic events calculated by the two equations, their standard deviations and the corresponding number of stations used to reach the final ML value. We called 'MLRI35' the magnitudes calculated by the Equation (1) and 'ML_Donegal' the magnitudes resulting from Equation (2). After a first magnitudes calculation, the values of ML_Donegal were substantially different from the mean MLRI35 values, with higher standard deviations. We then discarded the seismic stations D32 and D34 from the ML_Donegal calculation because they have lower S/N ratio and are the most distant from the epicentres. Finally, we come up with

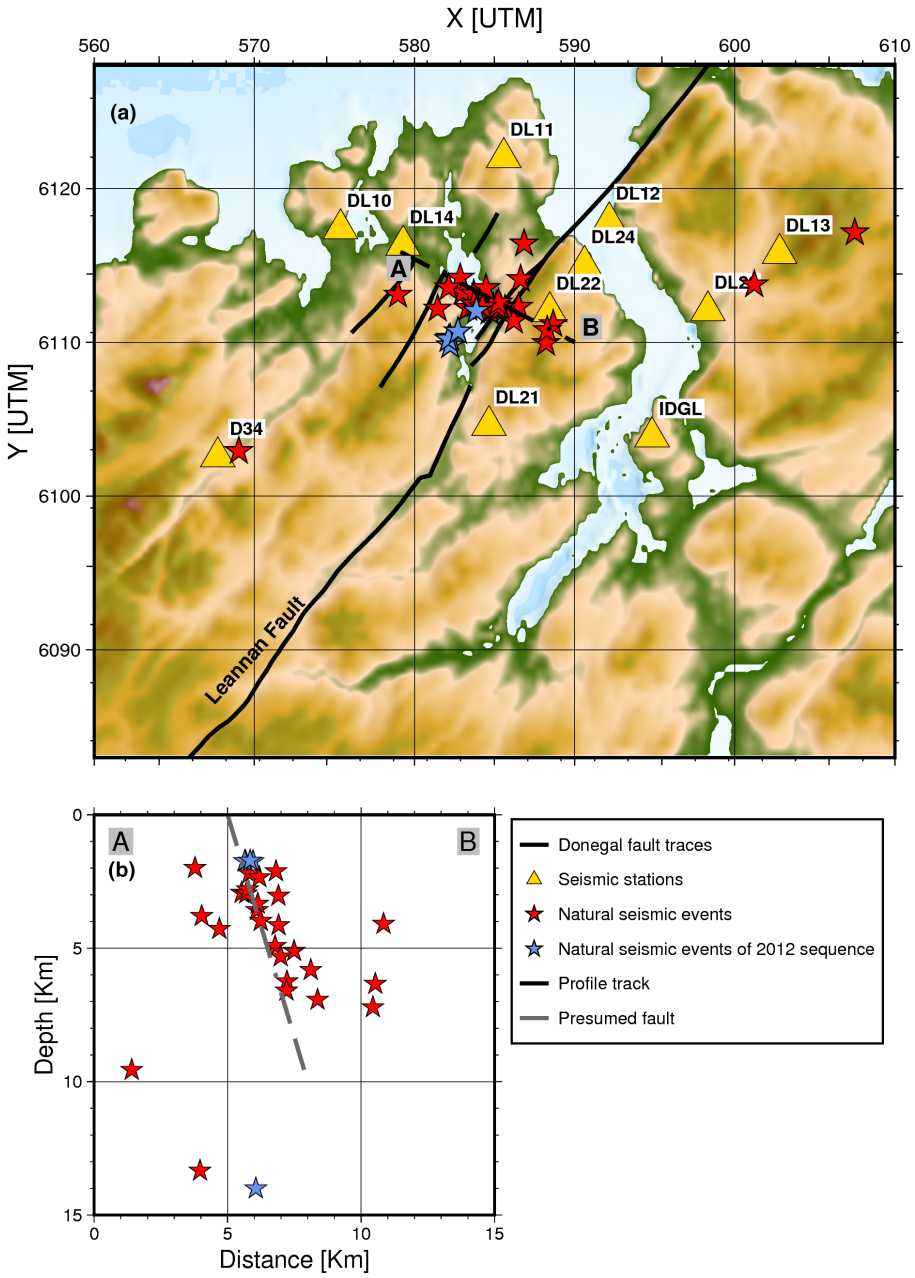

FIGURE 9 Natural seismic events plotted on the X-Y map and on the Z coordinate. Panel (a) shows the seismic stations and the track of the NW-SE profile. Panel (b) shows the natural events projected on depth and the presence of the presumed fault.

the magnitude values reported in Table 3. In some cases, the magnitudes calculated by Equation (2) are still slightly lower than the 'MLRI35' values. However, the majority of them are below 2 with small standard deviations and this result is in agreement with the magnitude values expected for Co. Donegal.

4 | DISCUSSION

The natural seismicity examined in this study is consistent with the tectonic setting of the region and, in particular, with the mapped NE-SW fault system (Figure 9a). The lower panel shows earthquakes plotted in cross-section. The majority of events shown in Figure occur along steeply SE dipping feature. The upward continuation of the represented tectonic feature could reach the Glen fault, a NE-SW trending sinistral strike-slip deformation widespread throughout the Highlands of Scotland and NW Ireland, that has been interpreted as a response to the subduction of Iapetus and continental collision (Kirkland et al., 2008). The southwestern continuation of the Great Glen Fault zone is marked in NW Ireland by the Leannan Fault (Figure 9) and the presumed fault marked in the cross-section Figure 9 (panel b) may be part of its splay. The Figure also shows that most earthquakes are located at depths of less than 10 km, with a few events occurring at greater depth. The depth distribution of the

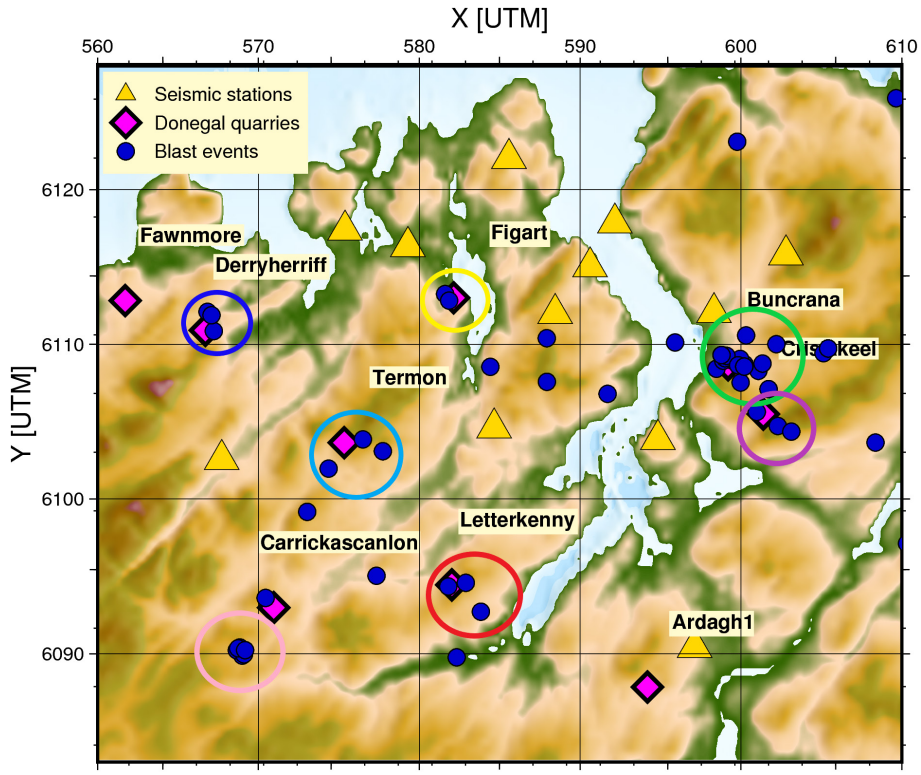

FIGURE 10 Blast events plotted on the X-Y plane. Clusters of events are related to local active quarries.

TABLE 1 Donegal quarries' names and coordinates referred to the clusters of blast represented in Figure 10.

Name	Latitude	Longitude
Buncrana Co-Donegal	55.116	−7.440
Termon Co-Donegal	55.072	−7.820
Derryherriff Co-Donegal	55.136	−7.958
Carrickascanlon Co-Donegal	54.978	−7.890
Crislakeel Co-Donegal	55.088	−7.405
Letterkenny Co-Donegal	54.991	−7.714
Figart Co-Donegal	55.154	−7.712

TABLE 2 Station correction coefficients.

Seismic station	Station correction coefficient
IDGL	0.207577
DL10	−0.445406
DL11	−0.150145
DL12	−0.445576
DL13	−0.115051
DL14	−0.293419
DL21	0.037369
DL22	−0.435984
DL23	−0.53154
DL24	−0.471261
DL31	−0.209358

earthquakes suggests that most events occur within the radiogenic granites buried at shallow depth. The presence of Donegal granites might have created a vulnerable zone in the Lennan Fault System, potentially contributing to its current seismic activity (Hensen et al., 2019).

The natural seismicity is gathered between 55.12 and 55.22 N in latitude and between −7.74 and −7.60 E in longitude (580–590 Km on the X coordinate and 6110–6120 Km on the Y coordinate) (Figure 9a), both for more recent and sparse seismic events and for a seismic sequence occurred in the area. This fact indicates that tectonic stress, in region of slow tectonic deformation, is still accommodated along pre-existent fault systems which behave as weak zone in the upper crust. Even if the (suggested) sources for such stress are located either far away (i.e. mid-Atlantic ridge, Hensen et al., 2019) or at the surface (i.e. post-glacial rebound Wu et al., 1999), seismic events pop-up in precisely defined zones, characterized by fault systems mapped at the surface and most probably inherited from previous geodynamic processes. Here, the process that led the development of the Great Glen fault, for which our study area is the southward continuation, was probably active mainly prior to the Upper Carboniferous (300 Ma, Kennedy, 1946). Nevertheless, present-day seismic activity still clusterizes along such weak zones.

TABLE 3 Magnitude values at each stations calculated by using Equation (1) ('MLRI35') and Equation (2) ('ML_Donegal'), their standard deviations and the corresponding number of station used to reach the final averaged ML value.

Idev_num	Idev	MLRI35	MLRI35_std	Num_sta_good	ML_Donegal	ML_Donegal_std	Num_sta_good
01	20,120,928,062,959	1.6	0.3	4	1.2	0.1	4
02	20,121,024,065,903	1.5	0.3	6	1.3	0.2	6
03	20,121,031,193,817	1.5	0.3	6	1.0	0.6	6
04	20,121,122,194,654	1.9	0.4	7	2.3	0.1	6
05	20,130,210,063,823	1.5	0.2	6	1.2	0.2	6
06	20,130,402,052,503	2.3	0.3	7	1.3	0.3	7
07	20,130,405,004,553	2.8	0.3	7	3.7	0.2	7
08	20,130,405,004,643	1.4	0.3	7	0.9	0.2	7
09	20,130,503,203,415	1.5	0.3	7	1.7	0.3	7
10	20,130,521,101,615	1.4	0.3	6	1.5	0.2	6
11	20,130,523,130,545	1.4	0.3	6	1.7	0.3	6
12	20,130,528,095,326	1.4	0.3	7	1.0	0.4	7
13	20,130,602,025,737	1.6	0.4	7	1.2	0.2	7
14	20,130,608,123,331	1.4	0.3	7	1.2	0.7	7
15	20,130,609,032,716	1.4	0.3	7	0.4	0.1	7
16	20,130,622,075,627	1.4	0.3	7	1.2	0.1	6
17	20,130,625,021,853	1.4	0.3	7	0.2	0.3	7
18	20,130,625,221,351	1.4	0.3	7	0.5	0.5	7
19	20,130,720,051,915	1.5	0.2	8	0.5	0.6	8
20	20,130,925,094,650	1.8	0.3	7	1.2	0.3	7
21	20,131,231,194,717	1.5	0.2	8	1.1	0.4	8
22	20,140,314,011,925	1.5	0.3	8	0.7	0.4	8
23	20,140,401,120,612	1.5	0.2	8	1.7	0.2	8
24	20,140,429,040,202	1.5	0.2	8	1.4	0.3	8
25	20,140,519,061,145	1.5	0.2	8	1.1	0.2	7
26	20,140,611,130,418	1.5	0.3	8	1.4	0.3	8
27	20,140,619,111,118	1.6	0.4	8	1.5	0.3	8
28	20,140,706,122,114	1.5	0.2	8	0.6	0.4	8
29	20,140,706,155,212	1.5	0.2	8	0.8	0.3	8
30	20,140,728,115,302	1.5	0.3	8	1.2	0.3	7
31	20,140,805,055,249	1.5	0.2	8	1.8	0.3	8
32	20,140,818,001,902	1.5	0.3	8	1.0	0.2	7
33	20,141,209,063,409	1.4	0.3	6	1.8	0.2	6
34	20,150,521,215,759	1.5	0.3	5	0.9	0.1	5
35	20,150,701,004,049	1.4	0.4	3	0.4	0.1	3

Finally, we observe a relevant number of seismic sources throughout the study area, not consistent with 'standard' natural seismic events (i.e. not consistent with shear events, with unclear or absent S-wave arrival and associated long-period coda waves). Such events have been associated to local human activities, mainly explosions in quarries. Such events form small local clusters in precise locations. Being the positions of the quarries know within a certain precision, such seismic sources could be in future used as 'active sources' for further crustal investigations.

5 | CONCLUSIONS

Seismic traces registered from August 2012 to June 2015 by stations of the Seismic network deployed in Donegal in the framework of the SIM-CRUST project and by two stations belonging to a previous temporary seismic network, ISLE/ISUME projects have been analysed to detect natural and anthropic seismicity, in a target area for future geothermal exploitation. The position of the located events indicate that:

1. Clusterized micro-seismicity is present with a magnitude generally lower than Mw = 1.0–2.0 (i.e. not felt by population)
2. Such events are localized within previously mapped fault systems in Co. Donegal.
3. Anthropogenic seismicity is widely recorded through the entire study area, and it is mostly related to quarries' activity in the studied area.

Through this work we produced the first manually revised catalogue of Donegal micro-seismicity and, more widely, of the entire Ireland. This kind of catalogues is fundamental for both getting new insights into the geodynamic processes on-going in regions of slow lithospheric deformation, and for future exploitation of geo-resources.

ACKNOWLEDGEMENTS

We would like to thank the Dublin Institute for Advanced Studies for sharing the seismic data. In particular, we are in debt with James Grannel for information about Donegal quarries, the discussion on the magnitude and event catalogue and the station correction coefficients, Martin Möllhoff for the maintenance of the seismic stations and the data archives. The seismic data analysed in this thesis have been collected during the SFI funded project SIM-CRUST Grant Number 11/SIRG/E2174 (https://sim-crust.dias.ie/). NPA thanks John O'Raw, Danny Mc Fadden, David Mc Gloin, Michelle Johnstone, Henry and Martin Callaghan, Henry McKinney, Gerard Mc Daid, Michael Tinney, Derek Flanagan and Dr Alessandro Amato for the deployment of the seismic network. Andrea Licciardi and Andrew Schaeffer helped in managing the seismic network in Donegal. Preliminary analysis of the quarry blasts recorded in Donegal has been done by Maite Zabaltza during her internship at DIAS.

DATA AVAILABILITY STATEMENT

Data will be available on Mendeley upon manuscript acceptance: https://data.mendeley.com/ Data link can be shared with reviewers upon request before manuscript acceptance.

ORCID

Federica Riva https://orcid.org/0000-0001-7400-0757

REFERENCES

Agostinetti, N. P., & Licciardi, A. (2015). *SIM-CRUST Project-Seismic Imaging and Monitoring of the Upper Crust: Exploring the Potential Low-Enthalpy Geothermal Resources of Ireland*. Citeseer.

Bayes, T. (1763). An essay towards solving a problem in the doctrine of chances. *Philosophical Transactions. Royal Society of London*, *53*, 370–418.

Billings, S. D., Kennett, B. L. N., & Sambridge, M. (1994). Hypocentre location: Algorithms incorporating problem-specific information. *Geophysical Journal International*, *118*, 693–706.

Bodin, T., Sambridge, M., Rawlinson, N., & Arroucau, P. (2012). Transdimensional tomography with unknown data noise. *Geophysical Journal International*, *189*, 1536–1556. https://doi.org/10.1111/j.1365-246X.2012.05414.x

Executable Books Community. (2021). Jupyter Book (v0.10). Zenodo. https://doi.org/10.5281/zenodo.4539666

Grannell, J., Arroucau, P., Lebedev, S., Moellhoff, M., & Bean, C. J. (2018). A Local Magnitude Scae for Ireland and its Offshore Regions, Poster Presentation, ESC General Assembly.

Goldstein, P., & Snoke, A. (2005). Sac availability for the iris community. *Incorporated Research Institutions for Seismology Newsletter*, *7*, 1–6.

Goodman, R., Jones, G. L., Kelly, J., Slowey, E., & O'Neill, N. (2004). Geothermal energy exploitation in Ireland – Review of current status and proposals for optimising future utilisation. CSA report 3085/02.04 for Sustainable Energy Ireland.

Hensen, C., Duarte, J. C., Vannucchi, P., Mazzini, A., Lever, M. A., Terrinha, P., Géli, L., Henry, P., Villinger, H., Morgan, J., Schmidt, M., Gutscher, M.-A., Bartolome, R., Tomonaga, Y., Polonia, A., Gràcia, E., Tinivella, U., Lupi, M., Çağatay, M. N., … Nuzzo, M. (2019). Marine transform faults and fracture zones: A joint perspective integrating seismicity, fluid flow and life. *Frontiers in Earth Science*, *7*, 1–29.

Kennedy, W. Q. (1946). The great Glen fault. *Quarterly Journal of the Geological Society*, *102*, 41–76.

Kirkland, C., Alsop, G., & Prave, A. (2008). The brittle evolution of a major strike-slip fault associated with granite emplacement: A case study of the leannan fault, nw Ireland. *Journal of the Geological Society*, *165*, 341–352.

Korrat, I., Lethy, A., ElGabry, M., Hussein, H., & Othman, A. S. (2022). Discrimination between small earthquakes and quarry blasts in Egypt using spectral source characteristics. *Pure and Applied Geophysics*, *179*, 599–618.

Lahr, J. C. (1989). HYPOELLIPSE: A computer program for determining local earthquake hypocentral parameters, magnitude, and first-motion pattern. Open-File Report 99-23, U.S. Geological Survey. http://pubs.usgs.gov/of/1999/ofr-99-0023/

Lomax, A., Michelini, A., & Curtis, A. (2009). *Earthquake location, direct, global-search methods* (pp. 2449–2473). Springer New York.

Lomax, A., Virieux, J., Volant, P., & Berge-Thierry, C. (2000). *Probabilistic earthquake location in 3D and layered models* (pp. 101–134). Springer Netherlands. https://doi.org/10.1007/978-94-015-9536-0_5

Malinverno, A., & Briggs, V. A. (2004). Expanded uncertainty quantification in inverse problems: Hierarchical bayes and empirical bayes. *Geophysics*, *69*, 1005–1016.

Metropolis, N., Rosenbluth, A. W., Rosenbluth, N. M., Teller, A. H., & Teller, E. (1953). Equation of state calculations by fast computing machines. *The Journal of Chemical Physics*, *1*, 1087–1092.

Möllhoff, M., & Bean, C. J. (2016). Seismic noise characterization in proximity to strong microseism sources in the Northeast Atlantic. *Bulletin of the Seismological Society of America*, *106*, 464–477. https://doi.org/10.1785/0120150204

Mosegaard, K. (2006). *Monte Carlo analysis of inverse problem*. Ph.D. thesis. Copenhagen University.

Mosegaard, K., & Tarantola, A. (1995). Monte carlo sampling of solutions to inverse problems. *Journal of Geophysical Research: Solid Earth*, *100*, 12431–12447.

Münchmeyer, J., Woollam, J., Rietbrock, A., Tilmann, F., Lange, D., Bornstein, T., Diehl, T., Giunchi, C., Haslinger, F., Jozinović, D., Michelini, A., Saul, J., & Soto, H. (2022). Which picker fits my data? A quantitative evaluation of deep learning based seismic pickers, *127*.

Piana Agostinetti, N., & Malinverno, A. (2015). Receiver function inversion by trans-dimensional Monte Carlo sampling. *Geophysical Journal International*, *181*, 858–872. https://doi.org/10.1111/j.1365-246X.2010.04530.x

Pitcher, W. S., Elwell, R. W. D., Tozer, C. F., & Cambray, F. W. (1964). The leannan fault. *Quarterly Journal of the Geological Society of London*, *120*, 241–270.

Readman, P. W., & O'Reilly, B. M. (2022). Ireland array. https://geofon.gfz-potsdam.de/doi/network/1M/2003

Richter, C. F. (1935). An instrumental earthquake magnitude scale*. *Bulletin of the Seismological Society of America*, *25*, 1–32. https://doi.org/10.1785/BSSA0250010001

Saadalla, H., Abdelhafiez, H., & Hayashida, T. (2023). Discrimination between earthquakes and quarry blasts in the Aswan region, southern Egypt, using p-wave source spectra. *Journal of Seismology*, *27*, 1–11.

Sambridge, M., & Mosegaard, K. (2002). Monte Carlo methods in geophysical inverse problems. *Reviews of Geophysics*, *40*, 1–29. https://doi.org/10.1029/2000RG000089

Somogyvári, M., & Reich, S. (2020). Convergence tests for transdimensional markov chains in geoscience imaging. *Mathematical Geoscience*, *52*, 651–668. https://doi.org/10.1007/s11004-019-09811-x

Tarantola, A. (2005). *Inverse problem theory and methods for model parameter estimation*. SIAM.

Team, T. O. D. (2017). Obspy 1.0.3. https://doi.org/10.5281/zenodo.165134

Theunissen, T., Chevrot, S., Sylvander, M., Monteiller, V., Calvet, M., Villaseñor, A., Benahmed, S., Pauchet, H., & Grimaud, F. (2017). Absolute earthquake locations using 3-D versus 1-D velocity models below a local seismic network: Example from the Pyrenees. *Geophysical Journal International*, *212*, 1806–1828. https://doi.org/10.1093/gji/ggx472

Waldhauser, F., & Ellsworth, W. (2000). A double-difference earthquake location algorithm: Method and application to the Northern Hayward fault, California. *Bulletin of the Seismological Society of America*, *90*, 1353–1368.

Wessel, P., Luis, J., Uieda, L., Scharroo, R., Wobbe, F., Smith, W., & Tian, D. (2019). The generic mapping tools version 6. *Geochemistry, Geophysics, Geosystems*, *20*, 5556–5564.

Wu, P., Johnston, P., & Lambeck, K. (1999). Postglacial rebound and fault instability in Fennoscandia. *Geophysical Journal International*, *139*, 657–670.

SUPPORTING INFORMATION

Additional supporting information can be found online in the Supporting Information section at the end of this article.

Data S1

Data S2

Data S3

Data S4

How to cite this article: Riva, F., Agostinetti, N. P., Marzorati, S., & Horan, C. (2023). The micro-seismicity of Co. Donegal (Ireland): Defining baseline seismicity in a region of slow lithospheric deformation. *Terra Nova*, *00*, 1–15. https://doi.org/10.1111/ter.12691

APPENDIX A

MONTE CARLO LOCATION OF SEISMIC EVENTS.

A. INTRODUCTION ON SEISMIC EVENT LOCATION

Here, we define a seismic event as a sudden release of elastic energy below the topographic surface, which produces seismic waves that propagate across the rock volume. Locating seismic events is a fundamental task for both monitoring the subsurface and studying the Earth's structure. A network of seismic stations at the surface (but also within the rock volume) can be used to locate such events, identifying the P and S waves arriving at the seismic stations, and measuring their arrival times t_p^o and t_s^o. Locating seismic events is a standard geophysical inverse problem (Tarantola, 2005), where seismologists indirectly measure the 3D position of a physical process (the seismic energy release) through the measure of related quantities (the arrival times of the seismic waves). Many different methodologies have been developed for solving such inverse problem, either based on linearized methodologies (e.g. Billings et al., 1994; Waldhauser & Ellsworth, 2000) or stochastic approaches (e.g. Lomax et al., 2009). Due to the need of modelling the propagation of the seismic waves, different workflows consider a 1D (e.g. Lahr, 1989) or 3D (e.g. Theunissen et al., 2017) Earth's model.

In this study, we develop a stochastic method based on a Markov chain Monte Carlo (McMC) sampling of parameters (Mosegaard & Tarantola, 1995). In stochastic methods, many randomly generated numerical representations of the physical model (i.e. the so-called *models*) are collected and, for each model, the predicted observations are generated (this operation is called *forward modelling* and the predictions are called *synthetics*). Through the comparison of synthetics and observations each single model is evaluated. Here, our physical model considers the existence of a homogeneous half-space which represents the rock volume and the seismic event can occur in any place of the rock volume itself with the same probability. To avoid bias given by mis-estimated uncertainties, we strictly follow a Hierarchical Bayes methodology Malinverno and Briggs (2004). The McMC sampling is guided by a Metropolis rule (Metropolis et al., 1953) and, thus, sampled solutions are used to make Bayesian inferences on the investigated parameters (e.g. estimating mean and standard deviation of each parameter, but also correlation between different parameters).

B. BACKGROUND ON BAYESIAN INFERENCES, MARKOV CHAIN MONTE CARLO AND HIERARCHICAL BAYES

Bayesian inferences is based on Bayes' theorem (Bayes, 1763):

$$P(\mathbf{m}|\,\mathbf{d}) = kP(\mathbf{m})L(\mathbf{m})\,, \tag{3}$$

where $\mathbf{m}$ is a model (i.e. a point in the model space), $\mathbf{d}$ is the vector of the observations, $P(\mathbf{m}|\,\mathbf{d})$ is the posterior probability distribution (see below), $P(\mathbf{m})$ is the prior probability distribution (see Section E), and $L(\mathbf{m})$ is the likelihood value (see Section D). Bayes' theorem is a probabilistic formula which relates a new state of knowledge (so-called

posterior probability distribution, PPD) on the investigated quantities (i.e. the model) with the previous state of knowledge (so-called *prior probability distribution* or simply prior) and a measure of the ability of the model itself to reproduce observations (so-called *likelihood function*). Bayesian inferences is a powerful tool for studying physical (and not-physical) parameters, because it is able to map out not only a single model which best reproduces the observations but also a wide family of models that explain the observation within a certain level.

Finding an analytic solution to Equation 3, however, could be impossible in a multidimensional space, especially in presence of complex prior probability distributions (i.e. not-Gaussian priors). In the last two decades, stochastic methods have been developed to overcome this issue, where the stochastic sampling of models is driven to sample the model space with a sampling frequency proportional to the target distribution (here the PPD, Sambridge & Mosegaard, 2002). Here, the adopt a McMC sampling strategy: a sequence of models (i.e. a chain) is collected according to some general rules. Let us assume to be in a position of the model space (called 'current model', $\mathbf{m}_{cur}$) and one more model is proposed for the chain (called 'candidate model', $\mathbf{m}_{cand}$). First, such model $\mathbf{m}_{cand}$ depends on the current model $\mathbf{m}_{cur}$ only, not on previously sampled models. This is the 'Markov' characteristic: a chain with the shortest possible memory. Second, the candidate model is accepted as next step in the chain according to the Metropolis rule: (1) it is always accepted if $L(\mathbf{m}_{cand}) \geq L(\mathbf{m}_{cur})$; or (2) it is accepted with a probability α if $L(\mathbf{m}_{cand}) < L(\mathbf{m}_{cur})$. Here, we follow the approach developed in Mosegaard and Tarantola (1995) and, thus, the probability α corresponds to the likelihood ratio, that is: $\alpha = L(\mathbf{m}_{cand}) / L(\mathbf{m}_{cur})$. Such formulation is valid only if the candidate model is proposed according to the priors (see Mosegaard & Tarantola, 1995, for details).

As described above, the likelihood function plays a key role in the McMC sampling. The Likelihood function (presented in details in Section D) depends on the data uncertainties. However, estimating errors in a set of measurements could be problematic and errors are sometimes over- or under-estimated. To avoid bias introduced by wrongly assumed measurement errors, we adopt a Hierarchical Bayes approach. In such approach, the data uncertainties are also considered as part of the unknowns and are estimated through the McMC sampling. This means that the model comprises both physical parameters representing the physical processes under investigation and not-physical parameters related to other aspect of the geophysical inverse problem (so-called 'hyper-parameters' Malinverno & Briggs, 2004). It has been noted by Bodin et al. (2012) that such hyper-parameters do not only estimate the data uncertainties themselves, but also account for the use of a simplified physical model and/or modelling (for example, in our case, the approximation for ray-paths as straight lines, see next section).

C. MODEL PARAMETERS AND FORWARD MODELLING

Our simplified model for the geophysical process of seismic wave propagation consists in a homogeneous half-space and a point-wise source from where the P and S waves originate. Given such description, our mathematical model is composed by eight parameters. Four parameters describe the event location in space and time. Two parameters represent the elasticity of the rock volume. The last two parameters are used to estimate the data uncertainties (separately for P and S arrival times). Thus, the model $\mathbf{m}$ can be written as:

$$\mathbf{m} = \left(x, y, z, t, V_P, V_S, \pi_P, \pi_S\right),$$

where (x, y, z, t) display event location, (V_P, V_S) indicate half-space elastic parameters, and (π_P, π_S) are used to scale data uncertainties.

The forward modelling, in our case, simulates the propagation of the seismic waves from the event source through the rock volume to the seismic stations. Given the assumption of an homogeneous rock volume, the ray-paths are straight lines and the synthetic arrival times can be computed as: $t^s_P(\mathbf{m}) = d / V_P + t$ and $t^s_S(\mathbf{m}) = d / V_S + t$, where d is the distance between the event in position (x, y, z) and one station in the seismic network. Regarding the data uncertainties, we assume a-priori a realistic value for the data variance σ_0^2 and we scale such variance with the hyper-parameters. So, the variance considered in the likelihood function (Section D) is: $\sigma^2(\mathbf{m}) = \sigma_0^2 \cdot 10^{2\pi_X}$, where X can be P or S.

D. LIKELIHOOD FUNCTION

The Likelihood function, for Gaussian distributed errors, can be written as:

$$L(\mathbf{m}) = p(\mathbf{d}|\,\mathbf{m}) = \frac{1}{\left(2\pi|\,C_e\right)^{1/2}} e^{-\frac{1}{2}\phi} \tag{4}$$

where ϕ represents the fit between model prediction $t^s_{X,i}$ and the i-th observation $t^o_{X,i}$, i.e. the residuals $\mathbf{e}_i = \left(t^s_{X,i} - t^o_{X,i}\right)$, with X being either P or S, through the covariance matrix of the error $C_\mathbf{e}$:

$$\phi = \mathbf{e}^T C_\mathbf{e}^{-1} \mathbf{e} \ . \tag{5}$$

In this study, we consider un-correlated errors in the measurements, thus $C_\mathbf{e}$ is a diagonal matrix with the data variance $\sigma^2(\mathbf{m})$ along the diagonal. In this case, accounting for the Hierarchical Bayes approach proposed, the likelihood function simplifies to:

$$L_X(\mathbf{m}) = \frac{1}{(2\pi)^{1/2}\sigma^N(\mathbf{m})} \exp \sum_i^N \left(\frac{t^s_{X,i}(\mathbf{m}) - t^o_{X,i}}{\sigma(\mathbf{m})} \right)^2 \tag{6}$$

with X being either P or S, N is the number of observations of phase X, and $L_X(\mathbf{m})$ the Likelihood for the X-wave arrival times. Obviously, being P- and S- wave arrival times un-correlated, the total likelihood for each model is given by the product of $L_P(\mathbf{m})$ by $L_S(\mathbf{m})$.

E. PRIORS

The definition of prior probability distributions is necessary to apply Bayesian inferences. Here we choose a uniform prior for all parameters. Uniform priors can be easily handled in computer codes and guarantee very loose constraints. The minimum and maximum values of all the priors are summarized in Table A1, together with the scale parameters (see section F).

TABLE A1 Prior distributions of model parameters in vector **m**.

Model parameter	Name	Minimum	Maximum	Scale
X coordinate	x	560 km	650 km	0.05
Y coordinate	y	6088 km	6128 km	0.05
Z coordinate	z	−20 km	0 km	0.15
T coordinate	t	−10 s	5 s	0.05
P-wave velocity	V_P	4.0 km/s	8.0 km/s	0.10
V_P / V_S ratio	V_P / V_S	1.5	1.9	0.20
Error on P-data	π_P	−0.5	5.0	0.075
Error on S-data	π_S	−0.5	5.0	0.075

F. RECIPE

A key-step in the McMC is the generation of a candidate model from the current model. There are several 'recipes' to generate a model starting from another model. In our study, we propose a candidate model in the following way. Staring from the current model, we randomly pick one of the perturbations listed below (called *moves*):

1. Modify the x coordinate (selected with probability 2 / 15);
2. Modify the y coordinate (2 / 15);
3. Modify the z coordinate (2 / 15);
4. Modify the t coordinate (2 / 15);
5. Modify the V_P value (2 / 15);
6. Modify the V_S value (2 / 15);
7. Modify the π_P and π_S values (3 / 15).

The perturbation will follow the scheme proposed in Appendix A in Piana Agostinetti and Malinverno (2010). Briefly, the algorithm will produce a sampling which asymptotically will sample the prior probability distribution. To guarantee an acceptance ratio of the McMC sampling between 0.1 and 0.5 (Mosegaard, 2006), each different move can be 'tuned' modifying the scale parameter introduced in Table A1.

F.1. TECHNICAL DETAILS

For each event, we run ten McMC samplings, collecting 100,000 models for each chain. Each chain is independent from the others and start from a different point of the parameter space (randomly selected). The McMC sampling can be processed on a personal computer or a dedicated server, with a limited CPU time (less than 30 s per event). In theory, each chain can be run in parallel on a computer cluster, to speed up the process in case of a large number of events (i.e. more than some hundreds of events). The first half of the collected models (500,000 models) is discarded because they are considered the 'burn-in' period (Somogyvári & Reich, 2020). We observe that the burn-in period should be generally more limited in this inverse problem, but we kept half of the sampling as a conservative choice. The second half of the sampled models is considered to be representative of the target PPD. To limit intra-chain correlation, we only retain 1/1000 of the sampled in the post burn-in phase. At the end we have a family of 500 models that are used to make inferences on the investigated parameters.